Analysis of the distortion of cantilever box girder with inner flexible diaphragms using initial parameter method

Yangzhi Ren[a,b*], Wenming Cheng[b], Yuanqing Wang[a], Bin Wang[c]

[a] Department of Civil Engineering, Tsinghua University, Beijing, China, 100084

[b] Department of Mechanical Enigneering, Southwest Jiaotong University, No.111, North Section 1, Second Ring Road, Chengdu, Sichuan, China, 610031

[c] College of Engineering, Design and Physical Sciences, Brunel University, London, Uxbridge UB8 3PH, UK.

[*]: Corresponding author

E-mail address: renyz66@mail.tsinghua.edu.cn ;

Abstract: In this paper, the distortion of cantilever box girders with inner flexible thin diaphragms is investigated under concentrated eccentric loads using initial parameter method (IPM), in which the in-plane shear strain of diaphragms is fully considered. A high-order statically indeterminate structure was established with redundant forces, where the interactions between the girder and diaphragms were indicated by a uniform distortional moment. Based on the compatibility condition between the girder and diaphragms, solutions for the distortional angle and the warping function were obtained by using IPM. The accuracy of IPM was well verified by finite element analysis for the distortion of cantilever box girders with 2, 5 and 9 diaphragms under three diaphragm thicknesses. Taking a lifting mechanism as an example, parametric studies were then performed to examine the effects of the diaphragm number and thickness, the ratio of height to span of the girder, the hook's location and the wheels' positions on the distortion of cantilever box girders. Numerical results were summarized into a series of curves indicating the distribution of distortional warping stresses and displacements for various cross sections and loading cases.

Keywords: cantilever girder; distortion; flexible diaphragm; initial parameter method; finite element analysis; shear deformation

Nomenclature

A, C = top and bottom flanges	t_1 t_2 = thickness of left and right webs
B, D = right and left webs	t_3 = thickness of flanges
B, *D* = total number of diaphragms and loads before the calculated point z	t_{pi} = thickness of ith diaphragm
$B_d(z)$ = distortional bimoment of cross section z	v = possion's ratio
b,h = width and height of girder	W_{add} = the additional distortional warping function
E= Young's elastic modular	$W(z)$ = distortional warping function
G = shear modular	x,y = in-plane coordinate axes of cross section
H_{ij}, V_{ij} = inner horizontal and vertical redundant forces	z = longitudinal axis of girder
$H(\alpha)$ = unit step function of variable α	z_j = location of jth concentrated load P_j
I_t, I_k , I_R = warping/polar/frame moment of inertia	z_{pi} = mid-line position of ith diaphragm

l = span of girder	$\boldsymbol{Z}(z)$ = state vector of cross section z in IPM
M, N, J, K = four angle nodes	β_d = ratio of warping stresses between nodes J and N
$M_d(z)$ = distortional moment of cross section z	γ_{pi} = in-plane shear strain of ith diaphragm
M_j = distortional moment produced by jth loads P_j	$\varphi_1, \varphi_2, \varphi_3, \varphi_4$ = combinations of trigonometric function
M_{pi} = distortional moment for ith diaphragm	λ_1, λ_2 = distortional coefficients of girder
m, n = total number of loads and diaphragms	θ = torsional angle of cross section
m_d = distributed distortional moment	$\chi(z)$ = distortional angle of cross section z
n_1,n_2 = distance between point O and webs	χ_{add} = the additional distortional angle
O = original point	τ_d = distortional shear stress
P_j = jth concentrated load	$\boldsymbol{\Phi}(z)$ = initial transfer matrix in IPM
$\boldsymbol{P}(z)$ = transfer matrix in IPM	$^{(1), (2), (3), (4), (i), (j)}$ = first, second, third, fourth, ith and jth differentiates
s = circumferential coordinate around profile	

1. Introduction

Cantilever box girders are widely applied in many cases. For instance, at container seaports, cantilever cranes are applied to handle containers from the boat to port (Fig.1a). In construction process, precast bridge segments are elevated and installed by cantilever cranes (Fig.1b). For cantilever girders subjected to eccentric loads, the flexure, torsion and distortion of the cross section are commonly concerned by designers. Both the warping deformation and stresses produced by distortional loads are usually so large that it may have significant values in comparison with the torsional and flexural ones.

(a) gantry crane (b) bridge construction

Fig.1 Examples of cantilever girders

In order to control the distortion of the beam cross section, diaphragms are installed at the interior of girders, which can increase not only the stability of local plate, but also the resistance to warping deformation and stresses [1,2]. The primary research on the distortion of girder has been performed using two methods - the Beam on Elastic Foundation (BEF) analogy [3] and the Equivalent Beam on Elastic Foundation (EBEF) analogy [4,5], where a thin diaphragm is analogous to simple supports and a thick solid diaphragm to fixed supports. Additionally, the effect of shear strain of the cross section on distortion is considered in EBEF analogy and cannot be ignored when the frame shear stiffness is significant to distortional warping one for box girders [6,7]. Since there is no clear boundary between the thin and thick diaphragms, it is difficult to accurately estimate the deformation and stresses of beams in BEF and EBEF methods when considering the thickness of diaphragms.

For a cantilever box girder with inner diaphragms, the key point of analyzing the deformation and stresses is to find out the interactions between the girder and diaphragms. A high-order statically indeterminate structure is modeled for girders with inner diaphragms under eccentric loads, where the interactions are indicated by redundant forces and moments [8-10], both are obtained from finite strip method [11] and force method [8]. This model is extensively researched on multi-span curved beams [12, 13]. Besides, an extended trigonometric series method [14] is applied to analyze the deformation and stresses of the girder with inner diaphragms, where webs and flanges are divided into several thin plates, and the thin-plate theory is applied to all members – flanges, webs and diaphragms. Interactions between the girder and diaphragms are indicated by compatibility conditions with respect to both displacements and forces. This method can achieve a high accuracy for both displacement and stresses, but the number of simultaneous equations is so large even for girders with few numbers of diaphragms that it is difficult to apply in practice. For example, there are up to 720 simultaneous equations for a girder with only two diaphragms.

Finite element analysis (FEA) is another important method for analyzing the distortion of the girder with inner diaphragms. Researchers evaluated the influence of the number of diaphragms on the deformation and stresses of straight [15-17], curved [18-20] and multi-cell [21,22] box girders with diaphragms by using FEA, where diaphragms were presumed to possess infinite in-plane shear stiffness and free warping for both torsion and distortion. Obviously, the assumption of infinite shear stiffness does not fit for girders with flexible thin diaphragms. Considering the finite in-plane shear stiffness of diaphragms, a distortional stiffness ratio is introduced [23] which is between the stiffness of various types of diaphragms over the stiffness of the solid-plate diaphragm. Both the type and location of diaphragms will make an influence on the horizontal loading distribution and to a less extent on the vertical one [24-26]. A research shows that orthogonal diaphragms are superior to skew ones in reducing the transversal bending stresses [27] and arranging the lateral loading distribution [28].

Initial parameter method (IPM), initially introduced to solve the non-uniform torsion of beams by Vlasov [29], has been extended to analyze the distortional deformation and stresses. In IPM, either the distortional angle or the warping function was taken as the original variable in the distortion equation [30-32], and the distortional deformation and stresses can be obtained according to the boundary conditions. High accuracy for both deformations and stresses produced by IPM has been verified by using FEA for girders without diaphragms. However, IPM has not been extensively applied to the distortion of girders with inner diaphragms. In addition, interactions between the girder and flexible thin diaphragms are still not clear in IPM.

Previous researches on girders with inner diaphragms has been generally performed under the assumption of infinite in-plane shear (distortional) stiffness, where the in-plane shear deformation of diaphragms was totally restrained and the out-of-plane warping deformation was free [15-22]. However, this assumption is not applicable to girders with flexible thin diaphragms [15, 18]. The main objective of this work is to analyze the distortion of cantilever girders with inner flexible thin diaphragms under eccentric loads, where the in-plane shear deformation of diaphragms is fully considered. Considering the compatibility between the girder and diaphragms, solutions for both the distortional deformations and stresses are obtained by using IPM. Numerical results are verified by applying FEA. Finally, taking a lifting mechanism as an example, a series of parametric studies are performed to examine the effects of the number and thickness of diaphragms, the hook's location and loading positions of trolley wheels on the distortion of cantilever girder with inner flexible diaphragms.

2. Structural model

Consider a cantilever box girder with inner diaphragms subjected to concentrated eccentric loads P_j (j=1, 2,…, m). The coordinate system O-xyz is illustrated in Fig.2a with its original point O

set at shear center of the cross section at the fixed end. For analysis, the distances between the point O and mid lines of webs B and D are marked by n_1 and n_2 in Fig.2b, respectively. The girder is made of a homogeneous, isotropic and linearly elastic material with the Young's and shear moduli E and G, respectively. The entire span is l. The thicknesses of webs B and D are t_1 and t_2 and the height is h, while the thicknesses of flanges A and C are t_3 and the width is b. The mid-line location of ith diaphragm, with the thickness being t_{pi}, is denoted as z_{pi} (i=1, 2,…,n) measured from the point O. The eccentric loads P_j are acted on the top of web D at z_j.

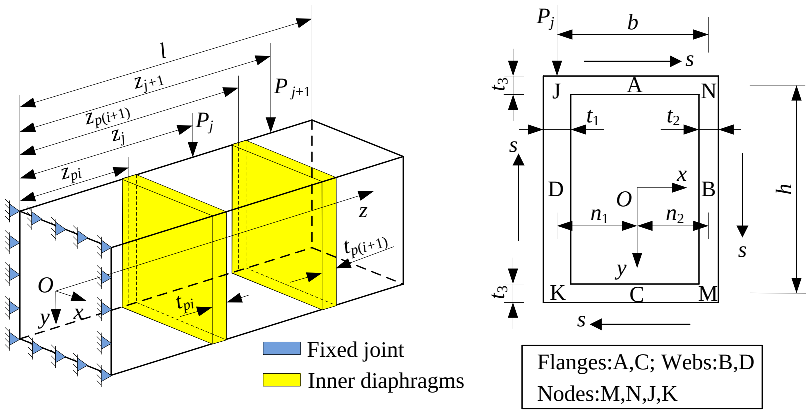

(a) cantilever girder with diaphragms (b) cross section

Fig.2 Cantilever box girder with diaphragms and its cross section

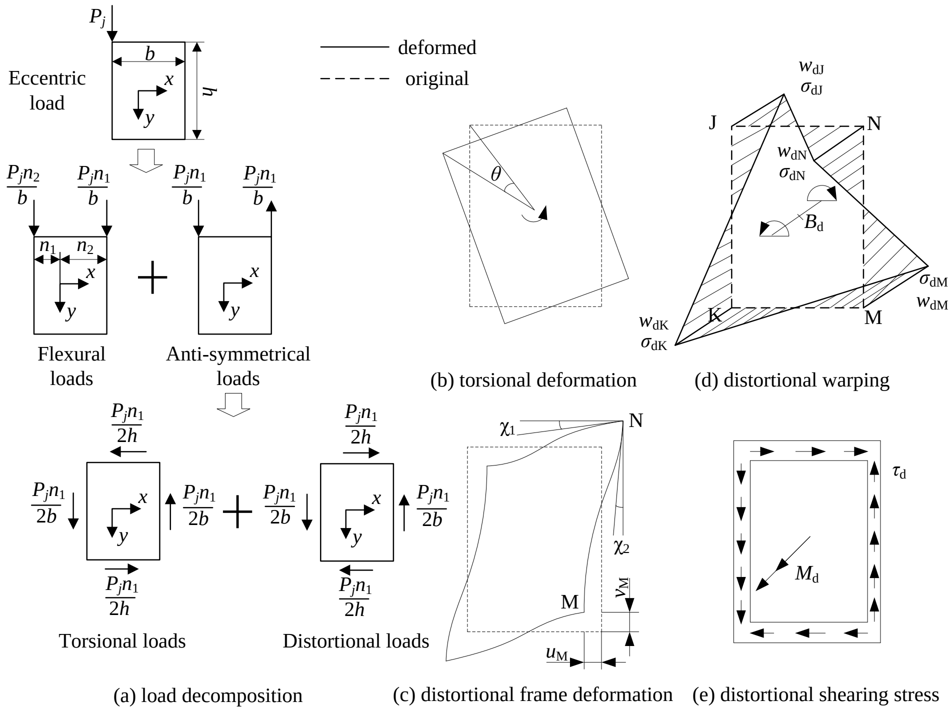

Fig.3 Loading decomposition, deformations and stresses of girders

Fig.3a shows that the load P_j can be decomposed into three components – flexural, torsional and distortional loads. In Fig.3b, the frame rigidly rotates around the point O with angle θ under torsional loads. In Fig.3c, both webs and flanges present transversal deflections under distortional loads, where u_M and v_M are horizontal and vertical in-plane displacements at node M, respectively. The variation of angle at node N is defined as the distortional angle χ, given by $\chi=\chi_1+\chi_2$. The warping displacements w_d and stresses σ_d, produced by distortional bimoment B_d, are illustrated in Fig.3d. Also, there exists shear stress τ_d in the cross-sectional profile, developed by distortional moment M_d, as shown in Fig.3e.

This paper will only focus on the distortional deformations and stresses of cantilever box girders with inner flexible thin diaphragms subjected to concentrated eccentric loads. That's also the deformations and stresses of cantilever box girders under concentrated distortional loads.

3. IPM for the distortion of cantilever box girder without diaphragms

In distortional analysis, the warping function $W(z)$ usually equals the first differentiate of angle $\chi(z)$. But when the shear stiffness has significant value in comparison with the warping one, the effect of shear strain of the cross section on deformations and stresses cannot be ignored [6,7]. The distortion equation is given by [6,7]

$$EI_t W^{(4)}(z) - \frac{EI_R EI_t}{GI_k} W^{(2)}(z) + EI_R W(z) = m_d^{(1)} \tag{1}$$

where m_d is the distributed distortional moment; the superscripts '(1), (2) and (4)' indicate the first, second and forth differentiates of $W(z)$ and m_d; I_t is the distortional warping moment of inertia, given by $I_t = \int_F \omega^2(s)\mathrm{d}F$, $\omega(s)$ is the sector coordinate, F is the cross-sectional area, s is the circumferential coordinate around the cross-sectional profile; I_k is the distortional polar moment of inertia, given by $I_k = \int_F \psi^2(s)\mathrm{d}F$, $\psi(s)$ is the generalized coordinate that describes the deformation in the s direction corresponding to a unit distortional angle; I_R is the distortional frame moment of inertia, given by $I_R = \int_F \left[\frac{\mathrm{d}^2\zeta(s)}{\mathrm{d}s^2}\right]^2 \frac{t^3}{12(1-v^2)}\mathrm{d}F$, $\zeta(s)$ is the deflection of the periphery of the profile in the direction normal to the s axis corresponding to a unit distortional angle; t is the thickness of the cross-sectional profile, and t=t_1 and t_2 for webs D and B, t=t_3 for flanges A and C;. v is the poisson's ratio.

Under concentrated distortional loads, m_d=0, and the solution for Eq.(1) is

$$W(z) = \sum_{i=1}^{4} B_i \varphi_i(z) \tag{2}$$

where B_i (i=1,2,3,4) are the parameters determined by boundary conditions, and the $\varphi_i(z)$ are:

$$\varphi_1(z)=\cosh(\lambda_1 z)\sin(\lambda_2 z),\ \varphi_2(z)=\cosh(\lambda_1 z)\cos(\lambda_2 z)$$

$$\varphi_3(z)=\sinh(\lambda_1 z)\cos(\lambda_2 z),\ \varphi_4(z)=\sinh(\lambda_1 z)\sin(\lambda_2 z)$$

where λ_i (i=1,2) is the distortional coefficients, given by

$$\lambda_1 = \frac{1}{2}\sqrt{\sqrt{\frac{4EI_R}{EI_t}} + \frac{EI_R}{GI_k}},\ \lambda_2 = \frac{1}{2}\sqrt{\sqrt{\frac{4EI_R}{EI_t}} - \frac{EI_R}{GI_k}}$$

Relations between the function $W(z)$ and the angle $\chi(z)$, the bimoment $B_d(z)$ and the moment $M_d(z)$ are [6,7]:

$$\chi(z) = -\frac{EI_t}{EI_R}W'''(z),\quad B_d(z) = -EI_t W',\quad M_d(z) = -EI_t W''. \tag{3}$$

Substitute Eq.(2) into Eq.(3), the matrix equation

$$\boldsymbol{Z}(z)=\boldsymbol{\Phi}(z)\boldsymbol{B} \tag{4}$$

is obtained, where

$$\boldsymbol{\Phi}(z)=\begin{bmatrix} -\frac{EI_t}{EI_R}\varphi_1'''(z) & -\frac{EI_t}{EI_R}\varphi_2'''(z) & -\frac{EI_t}{EI_R}\varphi_3'''(z) & -\frac{EI_t}{EI_R}\varphi_4'''(z) \\ \varphi_1(z) & \varphi_2(z) & \varphi_3(z) & \varphi_4(z) \\ \varphi_1'(z) & \varphi_2'(z) & \varphi_3'(z) & \varphi_4'(z) \\ \varphi_1''(z) & \varphi_2''(z) & \varphi_3''(z) & \varphi_4''(z) \end{bmatrix};\ \boldsymbol{B}=\{B_1, B_2, B_3, B_4\}^{\mathrm{T}};$$

$\boldsymbol{Z}(z)$ is the state vector of any section in IPM,

$$\boldsymbol{Z}(z)=\left\{\chi(z),\, W(z),\, -\frac{B_{\mathrm{d}}(z)}{EI_t},\, \frac{M_{\mathrm{d}}(z)}{EI_t}\right\}^{\mathrm{T}}. \tag{5}$$

The boundary conditions for cantilever girders are

$\chi(0)=0$, $W(0)=0$, for initial end $z=0$;

$B_{\mathrm{d}}(l)=0$, $M_{\mathrm{d}}(l)=0$, for ultimate end $z=l$.

Correspondingly, the state vectors are

$$\boldsymbol{Z}(0)=\left\{0,\, 0,\, -\frac{B_{\mathrm{d}}(0)}{EI_t},\, \frac{M_{\mathrm{d}}(0)}{EI_t}\right\}^{\mathrm{T}},\quad \boldsymbol{Z}(l)=\left\{\chi(l),\, W(l),\, 0,\, 0\right\}^{\mathrm{T}} \tag{6}$$

For $z=0$, $\boldsymbol{Z}(0)=\boldsymbol{\Phi}(0)\boldsymbol{B}$ and the inverse transformation is

$$\boldsymbol{B}=[\boldsymbol{\Phi}(0)]_{\mathrm{inv}}\cdot\boldsymbol{Z}(0) \tag{7}$$

where $[\boldsymbol{\Phi}(0)]_{\mathrm{inv}}$ is the inverse matrix of $\boldsymbol{\Phi}(0)$.

Then substitute Eq.(7) into Eq.(4), $\boldsymbol{Z}(z)$ can be expressed as

$$\boldsymbol{Z}(z)=\boldsymbol{P}(z)\cdot\boldsymbol{Z}(0) \tag{8}$$

where $\boldsymbol{P}(z)$ is the transfer matrix, given by $\boldsymbol{P}(z)=\boldsymbol{\Phi}(z)\cdot[\boldsymbol{\Phi}(0)]_{\mathrm{inv}}$.

Eq.(8) is the standard form of initial parameter method for distortion. Based on the relations between $\varphi_i(z)$ and its differentiations (see Eq.(A.1)~Eq.(A.3) in Appendix A), $\boldsymbol{P}(z)$ is simplified as:

$$\boldsymbol{P}(z)=\begin{bmatrix} -SC_1'''(z) & -KC_2'''(z) & -SKC_3'''(z) & KC_4'''(z) \\ \frac{S}{K}C_1(z) & C_2(z) & SC_3(z) & -C_4(z) \\ \frac{S}{K}C_1'(z) & C_2'(z) & SC_3'(z) & -C_4'(z) \\ -\frac{S}{K}C_1''(z) & -C_2''(z) & -SC_3''(z) & C_4''(z) \end{bmatrix} \tag{9}$$

where $S=\dfrac{1}{2\lambda_1^2+2\lambda_2^2}$, $K=\dfrac{EI_t}{EI_R}$, $C_1(z)=\dfrac{\varphi_3(z)}{\lambda_1}-\dfrac{\varphi_1(z)}{\lambda_2}$, $C_3(z)=\dfrac{3\lambda_1^2-\lambda_2^2}{\lambda_1}\varphi_3(z)-\dfrac{\lambda_1^2-3\lambda_2^2}{\lambda_2}\varphi_1(z)$, $C_2(z)=\varphi_2(z)-\dfrac{\lambda_1^2-\lambda_2^2}{2\lambda_1\lambda_2}\varphi_4(z)$, $C_4(z)=\dfrac{\varphi_4(z)}{2\lambda_1\lambda_2}$.

Besides, the jth eccentric load is indicated by a vector $\boldsymbol{Z}_j$ in IPM, given by

$$\boldsymbol{Z}_j=\left\{0,\, 0,\, 0,\, \frac{M_j}{EI_t}\right\}^{\mathrm{T}} \tag{10}$$

in IPM, where M_j is the distortional moment produced by the jth eccentric loads, given by $M_j=P_j\cdot n_1/2$ [32], n_1 is the distance between web D and point O (see Fig.2b).

4. IPM for the distortion of cantilever box girder with inner diaphragms

4.1. IPM solution

For analysis, a statically indeterminate structure is modeled with redundant forces acting along the junctions between the girder and diaphragms, as shown in Fig.4a. The horizontal and vertical redundant forces H_{ij} and V_{ij} are illustrated in zoomed picture, where the subscript i indicates webs and flanges, i=A,B,C,D (see Fig.2b) and j=2,3…,q. The small circles indicate the joints where the redundant forces are located.

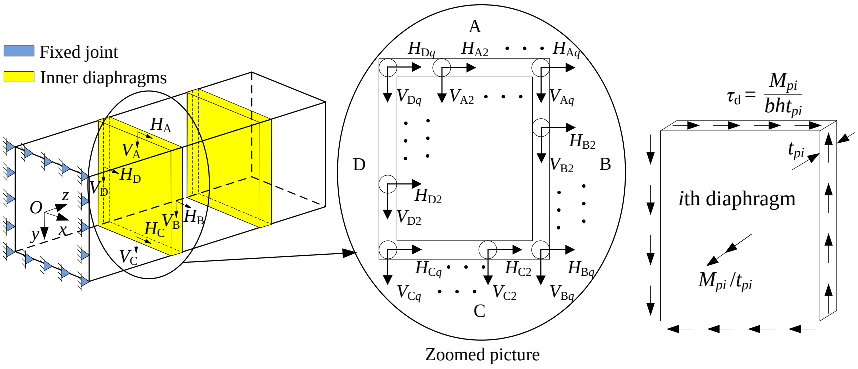

(a) a statically indeterminate structure (b) distortional boundary

Fig.4 High-order statically indeterminate structure

In order to analyze the interactions between the girder and diaphragms, two assumptions are made:

(1) Self balance assumption for in-plane forces of diaphragms

For diaphragms, summations of in-plane redundant forces and moments are all zeros under distortional loads. So only the distortional component of redundant force is reserved, as illustrated in Fig.4b. Furthermore, referred to the formation of the external moment M_j [32], all distortional components of redundant forces can be gathered and indicated by a moment M_{pi} for the ith diaphragm. So the interactions between the girder and diaphragms can be represented by the moment M_{pi}. The M_{pi}, in the direction opposite to M_j, will resist the warping deformation and stresses of the cross section. Similar to Eq.(10), the moment M_{pi} is indicated by the vector $\boldsymbol{Z}_{pi}$ in IPM, given by

$$\boldsymbol{Z}_{pi} = \left\{0,\ 0,\ 0,\ \frac{M_{pi}}{EI_t t_{pi}}\right\}^{\mathrm{T}}. \tag{11}$$

(2) Compatibility condition between the girder and diaphragms

The in-plane shear strain γ_{pi} of the ith diaphragm is considered, given by $\gamma_{pi} = M_{pi}/(Gbht_{pi})$, which is opposite to the distortional angle at the mid line of diaphragm. That is: $\chi(z_{pi}) = -\gamma_{pi}$ for $0 \leqq i \leqq n$. This is the key point to analyze the distortion of cantilever girders with diaphragms.

Combining Eq.(10) and Eq.(11) with Eq.(8), the vector $\boldsymbol{Z}(z)$ is given by

$$\boldsymbol{Z}(z) = \boldsymbol{P}(z)\boldsymbol{Z}(0) - \sum_{i=1}^{B} \int_{z_{pi}-t_{pi}/2}^{z_{pi}+t_{pi}/2} \boldsymbol{P}(z - z_i)\boldsymbol{Z}_{pi}\mathrm{d}z_i - \sum_{j=1}^{D} \boldsymbol{P}(z - z_j)\boldsymbol{Z}_j \tag{12}$$

where B and D are total numbers of diaphragms and eccentric loads before the calculated point z, respectively; z_{pi} is the mid-line location of the ith diaphragm (i=1,2,…, B); z_j is the location of the jth distortional loads (j=1,2,…, D); transfer matrices $\boldsymbol{P}(z–z_i)$ and $\boldsymbol{P}(z–z_j)$ are those obtained from $\boldsymbol{P}(z)$ by substituting the variable z by '$z–z_i$' and '$z–z_j$'.

For z=l, Eq.(12) changes into

$$\boldsymbol{Z}(l) = \boldsymbol{P}(l)\boldsymbol{Z}(0) - \sum_{i=1}^{n} \int_{z_{pi}-t_{pi}/2}^{z_{pi}+t_{pi}/2} \boldsymbol{P}(l - z_i)\boldsymbol{Z}_{pi}\mathrm{d}z_i - \sum_{j=1}^{m} \boldsymbol{P}(l - z_j)\boldsymbol{Z}_j \tag{13}$$

where $\boldsymbol{Z}(l)$ and $\boldsymbol{Z}(0)$ are matrices referred to Eq.(6).

Combining the third and forth equations in Eq.(13), $B_\mathrm{d}(0)$ and $M_\mathrm{d}(0)$ are obtained. Then, the angle $\chi(z)$ and function $W(z)$ are finally solved by substitute $B_\mathrm{d}(0)$ and $M_\mathrm{d}(0)$ into Eq.(12).

$$\chi(z)=\frac{\sum_{i=1}^{n}{}_B^1\eta_i(z)M_{pi}+\sum_{j=1}^{m}{}_D^1\varepsilon_{13}(z,z_j)M_j}{2\lambda_1\lambda_2 EI_R\Lambda_{13}(0,0)} \tag{14}$$

$$W(z)=\frac{\sum_{i=1}^{n}{}_B^2\eta_i(z)M_{pi}+\sum_{j=1}^{m}{}_D^2\varepsilon_{13}(z,z_j)M_j}{2\lambda_1\lambda_2 EI_t\Lambda_{13}(0,0)} \tag{15}$$

where the superscripts '1' and '2' in $\eta(z)$ and $\varepsilon(z, z_j)$ are related to the angle $\chi(z)$ and function $W(z)$. Similarly, the subscripts 'B' and 'D' are related to the values of B and D.

$$\begin{aligned}{}_B^1\eta_i(z)=&\frac{2}{t_{pi}}\left[\xi_{24}^{01}\left(l-z_{pi},\frac{t_{pi}}{2}\right)\Lambda_{13}^{31}(z,l)+\xi_{31}^{00}\left(l-z_{pi},\frac{t_{pi}}{2}\right)\Lambda_{31}^{32}(z,l)\right]\\&-H\left(B+\frac{1}{2}-i\right)\frac{2\Lambda_{13}(0,0)}{t_{pi}}\xi_{31}^{02}\left(z-z_{pi},\frac{t_{pi}}{2}\right)\end{aligned},$$

$$\begin{aligned}{}_B^2\eta_i(z)=&\frac{2}{t_{pi}}\left[\xi_{24}^{01}\left(l-z_{pi},\frac{t_{pi}}{2}\right)\Lambda_{13}^{10}(l,z)+\xi_{31}^{00}\left(l-z_{pi},\frac{t_{pi}}{2}\right)\Lambda_{31}^{20}(l,z)\right]\\&+H\left(B+\frac{1}{2}-i\right)\frac{2\Lambda_{13}(0,0)}{t_{pi}}\xi_{24}^{0(-1)}\left(z-z_{pi},\frac{t_{pi}}{2}\right)\end{aligned},$$

$${}_D^1\varepsilon_{13}(z,z_j)=\Gamma_{13}(z,z_j)-H\left(D+\frac{1}{2}-j\right)\varphi_4^{(3)}(z-z_j)\Lambda_{13}(0,0),$$

$${}_D^2\varepsilon_{13}(z,z_j)=\overline{\Gamma}_{31}(z,z_j)+H\left(D+\frac{1}{2}-j\right)\varphi_4(z-z_j)\Lambda_{13}(0,0),$$

where $H(\alpha)$ is a unit step function. Specifically, $H(\alpha)=1$ for $\alpha>0$; $H(\alpha)=0$ for $\alpha<0$. The superscripts '(1), (2), (3), (i) and (j)' is the first, second, third, ith and jth differentiates of functions $\varphi_n(\alpha)$ and $\varphi_m(\alpha)$.

$$\xi_{mn}^{ij}(\alpha,\beta)=\begin{vmatrix}\varphi_m^{(i)}(\alpha) & -\varphi_m^{(j)}(\beta)\\ \varphi_n^{(i)}(\alpha) & \varphi_n^{(j)}(\beta)\end{vmatrix},\quad \Lambda_{mn}^{ij}(\alpha,\beta)=\begin{vmatrix}\varphi_m^{(3)}(0) & \Phi_{4m}^{ij}(\alpha,\beta)\\ \varphi_n^{(3)}(0) & \Phi_{4n}^{ij}(\alpha,\beta)\end{vmatrix},\quad \Lambda_{ij}(\alpha,\beta)=\frac{\mathrm{d}^3\overline{\Lambda}_{ij}(\alpha,\beta)}{\mathrm{d}\alpha^3},$$

$$\Phi_{mn}^{ij}(\alpha,\beta)=\begin{vmatrix}\varphi_m^{(i)}(\alpha) & \varphi_m^{(j)}(\beta)\\ \varphi_n^{(i)}(\alpha) & \varphi_n^{(j)}(\beta)\end{vmatrix},\quad \overline{\Lambda}_{ij}(\alpha,\beta)=\begin{vmatrix}\varphi_i(\alpha) & \Phi_{4i}(l-\beta,l)\\ \varphi_j(\alpha) & \Phi_{4j}(l-\beta,l)\end{vmatrix},\quad \Phi_{ij}(\alpha,\beta)=\begin{vmatrix}\varphi_i^{(2)}(\alpha) & \varphi_j^{(2)}(\beta)\\ \varphi_i^{(1)}(\alpha) & \varphi_j^{(1)}(\beta)\end{vmatrix},$$

$$\overline{\Gamma}_{ij}(\alpha,\beta)=\begin{vmatrix}\varphi_i^{(3)}(0) & \overline{\Lambda}_{4i}(\alpha,\beta)\\ \varphi_j^{(3)}(0) & \overline{\Lambda}_{4j}(\alpha,\beta)\end{vmatrix},\quad \Gamma_{ij}(\alpha,\beta)=\frac{\mathrm{d}^3\overline{\Gamma}_{ij}(\alpha,\beta)}{\mathrm{d}\alpha^3};$$

In calculation, $\varphi_n^{(-1)}(\alpha)$ is the integral of $\varphi_n(\alpha)$, given by

$$\varphi_2^{(-1)}(\alpha)=\frac{\lambda_1\varphi_3(\alpha)+\lambda_2\varphi_1(\alpha)}{\lambda_1^2+\lambda_2^2},\quad \varphi_4^{(-1)}(\alpha)=\frac{\lambda_1\varphi_1(\alpha)-\lambda_2\varphi_3(\alpha)}{\lambda_1^2+\lambda_2^2}.$$

Besides, when the calculated point z is located in the thickness of (B+1)th diaphragm ($z_{p(B+1)}-t_{p(B+1)}/2\leqq z\leqq z_{p(B+1)}+t_{p(B+1)}/2$), the additional χ_add and W_add should be involved.

$$\chi_{\text{add}} = \frac{M_{p(B+1)}}{2\lambda_1\lambda_2 EI_R t_{p(B+1)}}\left[2\lambda_1\lambda_2 - \varphi_4^{(2)}\left(z - z_{p(B+1)} + \frac{t_{p(B+1)}}{2}\right)\right] \tag{16}$$

$$W_{\text{add}} = \frac{M_{p(B+1)}}{2\lambda_1\lambda_2 EI_t t_{p(B+1)}}\varphi_4^{(-1)}\left(z - z_{p(B+1)} + \frac{t_{p(B+1)}}{2}\right) \tag{17}$$

where $z_{p(B+1)}$, $t_{p(B+1)}$ and $M_{p(B+1)}$ are the mid-line location, thickness and distortional moment for (B+1)th diaphragm, respectively.

Obviously, from Eqs.(14)~(17), both the angle $\chi(z)$ and function $W(z)$ are related to moments M_j and M_{pi}. Since the moment M_j has been given in Eq.(10), the solutions rest in M_{pi}.

4.2. Derivation of M_{pi}

Based on the compatibility condition, compatibility equation is given by (T=1,2,…,n)

$$\frac{\sum_{i=1}^{n} {}_T^1\eta_i(z_{pT})M_{pi} + \sum_{j=1}^{m} {}_T^1\varepsilon_{13}(z_{pT}, z_j)M_j}{2\lambda_1\lambda_2 EI_R \Lambda_{13}(0,0)} + \frac{M_{pT}\left[2\lambda_1\lambda_2 - \varphi_4^{(2)}(t_{pT}/2)\right]}{2\lambda_1\lambda_2 EI_R t_{pT}} = -\frac{M_{pT}}{Gbht_{pT}} \tag{18}$$

where

$$\begin{aligned} {}_T^1\eta_i(z_{pT}) = {} & \frac{2}{t_{pi}}\left[\xi_{24}^{01}\left(l - z_{pi}, \frac{t_{pi}}{2}\right)\Lambda_{13}^{31}(z_{pT}, l) + \xi_{31}^{00}\left(l - z_{pi}, \frac{t_{pi}}{2}\right)\Lambda_{31}^{32}(z_{pT}, l)\right] \\ & - H\left(T - \frac{1}{2} - i\right)\frac{2\Lambda_{13}(0,0)}{t_{pi}}\xi_{31}^{02}\left(z_{pT} - z_{pi}, \frac{t_{pi}}{2}\right) \end{aligned},$$

$${}_T^1\varepsilon_{13}(z_{pT}, z_j) = \Gamma_{13}(z_{pT}, z_j) - H\left(k_T + \frac{1}{2} - j\right)\varphi_4^{(3)}(z_{pT} - z_j)\Lambda_{13}(0,0),$$

k_T is the number of eccentric loads before the T th diaphragm.

Correspondingly, the matrix equation system for Eq.(18) is

$$\boldsymbol{\eta}\cdot\boldsymbol{M}_p + \boldsymbol{\varepsilon} = \boldsymbol{0} \tag{19}$$

where

$$\boldsymbol{\eta} = \begin{bmatrix} R_{11} & {}_T^1\eta_2(z_{p1}) & {}_T^1\eta_n(z_{p1}) \\ {}_T^1\eta_1(z_{p2}) & R_{22} & \cdots\ {}_T^1\eta_n(z_{p2}) \\ \cdots & \cdots & \cdots \\ {}_T^1\eta_1(z_{pn}) & {}_T^1\eta_2(z_{pn}) & R_{nn} \end{bmatrix}, \boldsymbol{M}_p = \left\{M_{p1}, M_{p2}, \ldots, M_{pn}\right\}^T,$$

$$\boldsymbol{\varepsilon} = \left\{\sum_{j=1}^{m} {}_T^1\varepsilon_{13}(z_{p1}, z_j)M_j, \sum_{j=1}^{m} {}_T^1\varepsilon_{13}(z_{p2}, z_j)M_j, \ldots, \sum_{j=1}^{m} {}_T^1\varepsilon_{13}(z_{pn}, z_j)M_j\right\}^{\mathrm{T}},$$

and the diagonal element in the matrix $\boldsymbol{\eta}$ is

$$R_{ii} = {}_T^1\eta_i(z_{pi}) - \frac{\Lambda_{13}(0,0)}{t_{pi}}\left[\varphi_4^{(2)}\left(\frac{t_{pi}}{2}\right) - 2\lambda_1\lambda_2\left(1 + \frac{EI_R}{Gbh}\right)\right].$$

Then the moment M_{pi} is obtained based on the Cramer rule, given by

$$M_{pi} = -\sum_{j=1}^{m} Q_{ij}M_j \tag{20}$$

where $Q_{ij}=|\boldsymbol{\eta}_i|/|\boldsymbol{\eta}|$; the '$|\boldsymbol{\eta}|$' indicates the determinant of the matrix $\boldsymbol{\eta}$; For the matrix $\boldsymbol{\eta}_i$, all columns keep the same with the $\boldsymbol{\eta}$ except for the ith column [${}_T^1\varepsilon_{13}(z_{p1},z_j)$, ${}_T^1\varepsilon_{13}(z_{p2},z_j)$,…, ${}_T^1\varepsilon_{13}(z_{pn},z_j)$]^T.

4.3. Simplification for $\chi(z)$ and $W(z)$

Substitute Eq.(20) into Eq.(14), and the angle $\chi(z)$ changes into

$$\chi(z)=\frac{\sum_{i=1}^{n}\sum_{j=1}^{m}\left(\frac{{}_D^1\varepsilon_{13}(z,z_j)}{n}-{}_B^1\eta_i(z)Q_{ij}\right)M_j}{2\lambda_1\lambda_2 EI_R\Lambda_{13}(0,0)} \tag{21}$$

where m and n are the total numbers of distortional loads and diaphragms, respectively.

The number of calculation steps in Eq.(21) is $m\times n$, which is time-consuming for girders with many diaphragms under lots of loads. So a matrix equation system is established, given by

$$\boldsymbol{\eta}\cdot\boldsymbol{x}=\boldsymbol{\gamma} \tag{22}$$

where the matrix $\boldsymbol{\eta}$ is referred to Eq.(19); the matrices $\boldsymbol{x}$ and $\boldsymbol{\gamma}$ are

$$\boldsymbol{x}=\begin{Bmatrix} x_{11} & x_{12} & & x_{1n} \\ x_{21} & x_{22} & \cdots & x_{2n} \\ \cdots & \cdots & & \cdots \\ x_{n1} & x_{n2} & & x_{nn} \end{Bmatrix};\quad \boldsymbol{\gamma}=\begin{Bmatrix} \gamma_{11} & \gamma_{12} & & \gamma_{1n} \\ \gamma_{21} & \gamma_{22} & \cdots & \gamma_{2n} \\ \cdots & \cdots & & \cdots \\ \gamma_{n1} & \gamma_{n2} & & \gamma_{nn} \end{Bmatrix},$$

where the element $\gamma_{gk}=\begin{cases}\sum_{j=1}^{m}\left[{}_D^1\varepsilon_{13}(z,z_j){}_T^1\eta_k(z_{pg})/n-{}_B^1\eta_k(z){}_T^1\varepsilon_{13}(z_{pg},z_j)\right]M_j & (g\neq k)\\ \sum_{j=1}^{m}\left[{}_D^1\varepsilon_{13}(z,z_j)R_{gg}/n-{}_B^1\eta_k(z){}_T^1\varepsilon_{13}(z_{pg},z_j)\right]M_j & (g=k)\end{cases}$

In this way, the numerator of the angle $\chi(z)$ in Eq.(21) is transferred to the summation of diagonal elements in matrix $\boldsymbol{x}$. And the angle is expressed as

$$\chi(z)=\frac{1}{2\lambda_1\lambda_2 EI_R\Lambda_{13}(0,0)}\sum_{i=1}^{n}x_{ii} \tag{23}$$

Similar to the solution $\chi(z)$ in Eq.(23), the function $W(z)$ is given by

$$W(z)=\frac{1}{2\lambda_1\lambda_2 EI_t\Lambda_{13}(0,0)}\sum_{i=1}^{n}x_{ii} \tag{24}$$

where the element $\gamma_{gk}=\begin{cases}\sum_{j=1}^{m}\left[{}_D^2\varepsilon_{13}(z,z_j){}_T^1\eta_k(z_{pg})/n-{}_B^2\eta_k(z){}_T^1\varepsilon_{13}(z_{pg},z_j)\right]M_j & (g\neq k)\\ \sum_{j=1}^{m}\left[{}_D^2\varepsilon_{13}(z,z_j)R_{gg}/n-{}_B^2\eta_k(z){}_T^1\varepsilon_{13}(z_{pg},z_j)\right]M_j & (g=k)\end{cases}$.

Taking the node N as an example, the distortional warping displacement w_N, stress σ_N and shear stress τ_N can be obtained [33], given by

$$w_{dN}(z)=-\frac{bhW(z)}{4(\beta_d+1)},\quad \sigma_{dN}(z)=-\frac{EbhW^{(1)}(z)}{4(\beta_d+1)},\quad \tau_{dN}(z)=\frac{Ebh(h-b)W^{(2)}(z)}{96} \tag{25}$$

where β_d is the ratio of distortional warping stresses between the nodes J and N, $\beta_d=\frac{3bt_3+ht_1}{3bt_3+ht_2}$.

5. Verifications with FEA

In order to verify the accuracy of IPM, cantilever box girders with 2, 5 and 9 diaphragms are investigated under three diaphragm thicknesses by using FEA software package ANSYS. In the FEA model, Young's modulus E=210GPa, Poisson's ratio υ=0.3, the span l=1m, width b=0.1m, height h=0.2m and the flanges and webs thickness t=0.01m. Diaphragms are uniformly distributed along the span, with the thickness t_p being 0.005m, 0.01m and 0.02m, respectively.

Figs.5a, b and c give the mesh condition for cantilever girders with inner diaphragms using four-node element Shell63, where all DOFs are restrained on the fixed end. Convergence tests show that 1650 elements are appropriate for girders with two diaphragms, 1942 for those with five diaphragms and 2026 for those with nine diaphragms under the element size of 0.02m. Two concentrated distortional loads are applied at the cross sections z_1=0.45l and z_2=0.55l, including two horizontal components P_{h} (P_{h}=1.25 kN) on flanges and two vertical ones P_{v} (P_{v}=2.5 kN) on webs, as shown in Fig.5d.

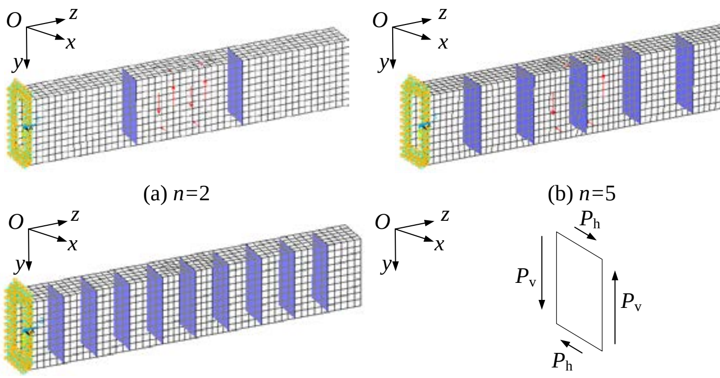

(a) n=2 (b) n=5 (c) n=9 (d) loading application

Fig.5 Meshing grid and loading application

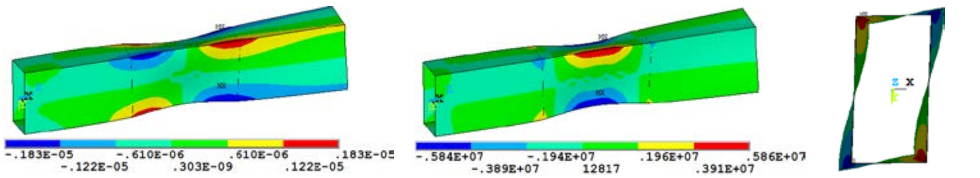

(a) warping displacement (b) warping stress (c) frame deformation

Fig.6 3D contours of cantilever box girder with 2 diaphragms under distortional loads (amp=3000)

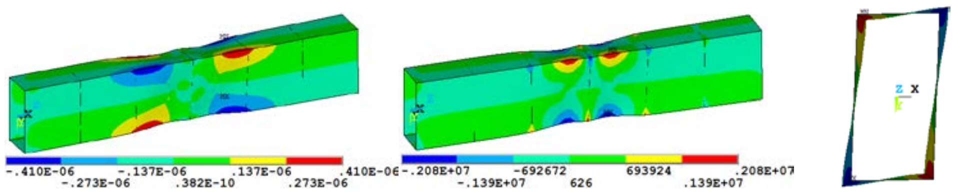

(a) warping displacement (b) warping stress (c) frame deformation

Fig.7 3D contours of cantilever box girder with 5 diaphragms under distortional loads (amp=10000)

Fig.6~Fig.8 give the 3D contours of warping displacements and stresses for cantilever box girders with 2,5 and 9 diaphragms, in which t_p=0.01m. The 'amp' indicates the amplified factor of deformations. It is seen that the largest warping displacement and stress both occur at the junctions between webs and flanges at the loading sections. With the increment of the diaphragm number, the largest warping stress reduces from 5.86Mpa to 1.55Mpa and displacement from 1.83μm to 0.268μm, and the frame deformation on the free end obviously become small.

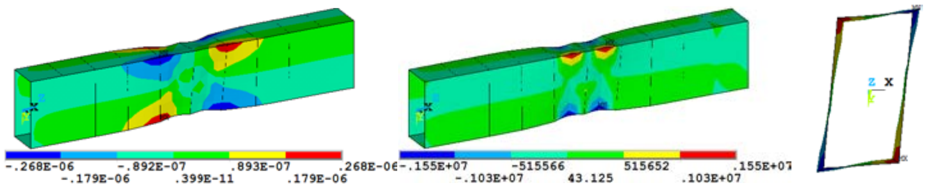

(a) warping displacement (b) warping stress (c) frame deformation

Fig.8 3D contours of cantilever box girder with 9 diaphragms under distortional loads (amp=20000)

Fig.9~Fig.11 give the comparison results between IPM and FEA for the distortional angle, warping displacement and stresses of cantilever box girders with 2,5 and 9 diaphragms, respectively. Each subplot includes three groups of curves and dots, divided by three thicknesses t_p/t=0.5, 1 and 2. The distortional angle in FEA model is calculated by the transversal displacements at nodes J, N and M (see Fig.2b).

$$\chi(z) = \frac{\mathrm{UX_N} - \mathrm{UX_M}}{h} + \frac{\mathrm{UY_N} - \mathrm{UY_J}}{b} \tag{26}$$

where $\mathrm{UX_N}$ and $\mathrm{UX_M}$ are x-axial displacements at nodes N and M, respectively; $\mathrm{UY_J}$ and $\mathrm{UY_N}$ are y-axial displacements at nodes J and N, respectively.

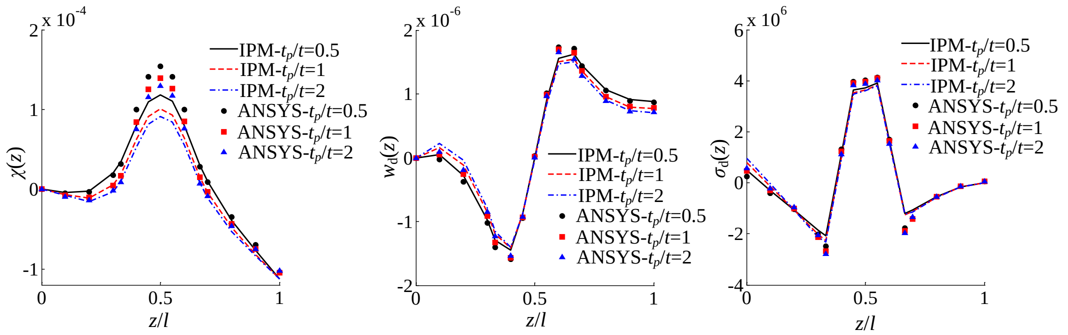

(a) angle $\chi(z)$ (b) warping displacement $w_d(z)$ (c) warping stress $\sigma_d(z)$

Fig.9 Comparisons of distortional angle, warping displacements and stresses between IPM and FEA for cantilever girders with two diaphragms under three diaphragm thicknesses

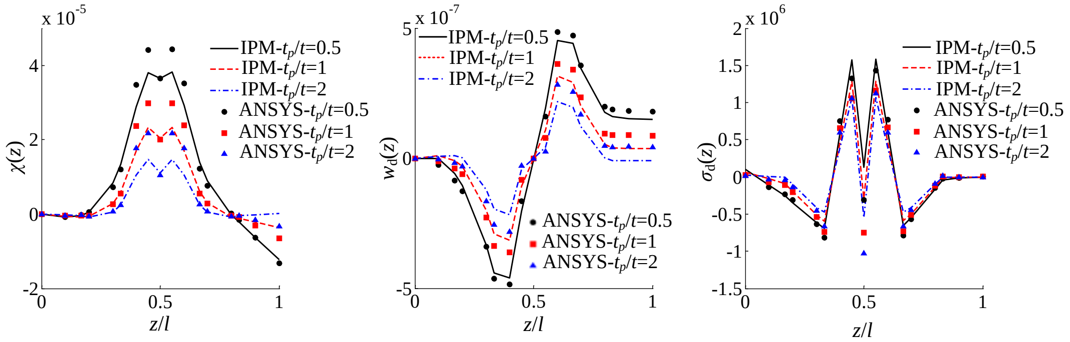

(a) angle $\chi(z)$ (b) warping displacement $w_d(z)$ (c) warping stress $\sigma_d(z)$

Fig.10 Comparisons of distortional angle, warping displacements and stresses between IPM and FEA for cantilever girders with five diaphragms under three diaphragm thicknesses

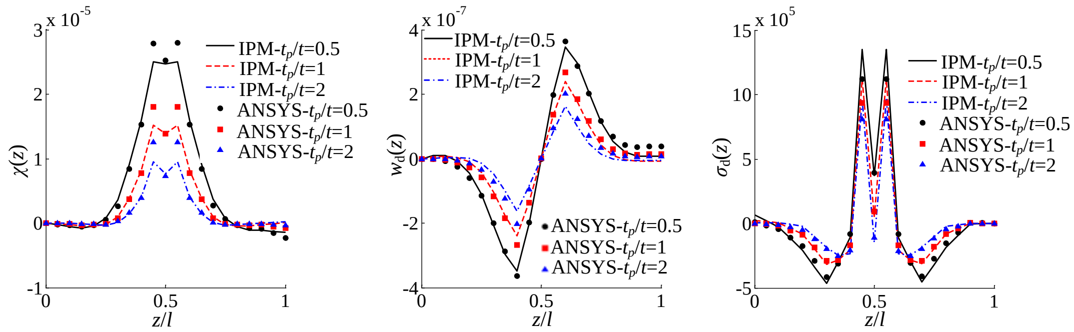

(a) angle $\chi(z)$ (b) warping displacement $w_d(z)$ (c) warping stress $\sigma_d(z)$

Fig.11 Comparisons of distortional angle, warping displacements and stresses between IPM and FEA for cantilever girders with nine diaphragms under three diaphragm thicknesses

Some findings can be drawn from Fig.9~Fig.11 as follows:

(1) Good agreements between IPM and FEA are evident for the distortional angle, warping displacement and stress of cantilever box girders with inner diaphragms, which well verifies the two aforementioned assumptions.

(2) The diaphragm thickness cannot be ignored, since the differences between girders with thin flexible diaphragms and thick solid ones become evident with the increment of the diaphragm number.

(3) Compared the girders strengthened by 2 diaphragms with those by 5 or 9 ones, it's worth being noted that the mid diaphragm effectively restrains the transversal deformation of the cross section at midspan.

(4) The largest error of distortional angles between IPM and FEA occurs at loading sections, where the FEA result is 20% larger than the IPM one for girders with two diaphragms (Fig.9a). However, this error reduces to 13.9% for girders with five diaphragms (Fig.10a) and 10.9% for those with nine diaphragms (Fig.11a). Since there is no diaphragms or stiffeners at the loading sections z_1=0.45l and z_2=0.55l, the error between IPM and FEA can be attributed to the local stress concentration. So the distortional angle obtained from IPM is susceptible to the influence of stress concentration, and it is necessary to install more diaphragms at the loading sections.

6. Parametric study

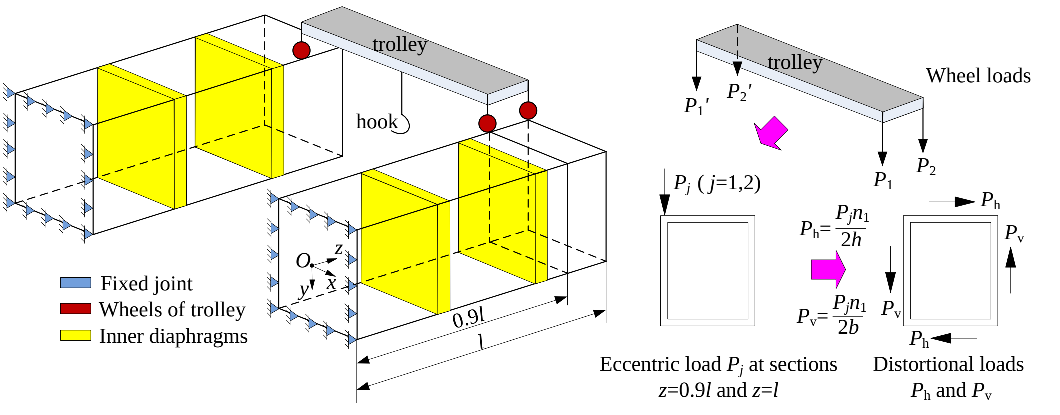

(a) moving lifting mechanism (b) distortional loads extracted from eccentrical loads

Fig.12 Lifting mechanism and the eccentric wheel loads

As shown in Fig.12a, a lifting mechanism model, including two girders and one trolley, is applied to investigate the effect of the diaphragm number and thickness on the distortion of cantilever girders. For simplicity, the measurements are set as t_1=t_2=t_3=t, t/b=0.1 and b/l=0.1.

Diaphragms are distributed uniformly in the span. As shown in Fig.12b, eccentric loads P_j and P_j' (j=1, 2) on trolley wheels are located at the cross sections z=0.9l and z=l, and only the distortional deformations and stresses are studied in this section.

Based on the IPM, four quantities - distortional angle, warping displacement and stress, shear stress are analyzed with respect to the diaphragm number and thickness, the ratio of height to span of the girder, the hook's location and the trolley wheels' position. Specifically, the effects of the diaphragm number and thickness, the ratio of height to span of the girder on four distortional quantities are considered in *Case* I, followed by the hook's location in *Case* II and the wheels' positions in *Case* III.

6.1. Case I

Taking the node N (see Fig.2b) of the cross section z=0.95l as an example, relationships between the four quantities and the diaphragm number n are summarized in Fig.13 varying with the ratio h/l of height to span of the girder, where t_p=t and P_1=P_2. The 'R-χ', 'R-w_d', 'R-σ_d', 'R-τ_d' represent the non-dimensional values of distortional angle, warping displacement and stress, shear stress of cantilever girders with inner diaphragms over those without diaphragms, respectively.

Some findings can be drawn from Fig.13 as follows

(1) In Fig.13a, the distortional angle reduces exponentially with the increment of the diaphragm number. The descending tendency is initially remarkable and then slows down when n>5, especially for girders with smaller ratio h/l. The warping displacement has the similar variability except for the girder with h/l=0.1, where its apex occurs at n=4, as shown in Fig.13b.

(2) Both the non-dimensional warping stress and shear stress are larger than 1 and increase exponentially with the diaphragm number. The ascending tendency is initially remarkable and then slow down when n>4, especially for girders with smaller ratio h/l, as shown in Fig.13c and d.

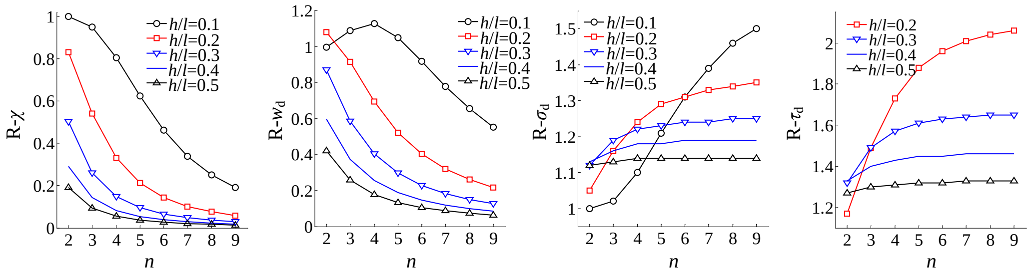

(a) distortional angle (b) warping displacement (c) warping stress (d) shearing stress

Fig.13 Relationships between four distortional quantities and the diaphragm number n varying with the ratio of height to span h/l

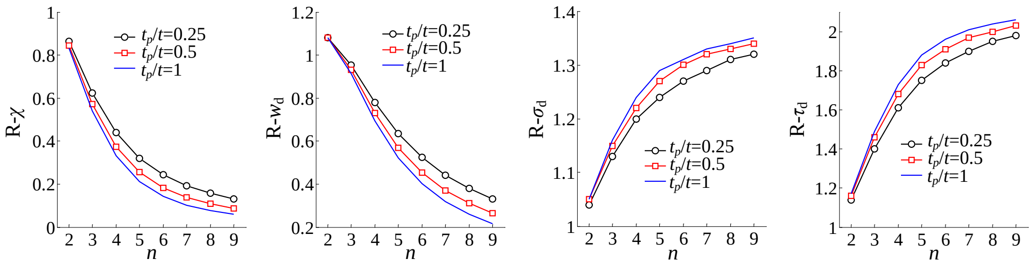

(a) distortional angle (b) warping displacement (c) warping stress (d) shearing stress

Fig.14 Relationships between four distortional quantities and the diaphragm number n varying with the thickness ratios t_p/t

Four quantities are also analyzed in Fig.14 varying with the ratio t_p/t of thicknesses between diaphragms and the girder, where h/l=0.2 and P_1 =P_2.

Some findings can be drawn from Fig.14 as follows

(1) In Fig.14a and b, the distortional angle and warping displacement reduce exponentially with the increment of the diaphragm number. The descending tendency is initially remarkable and then slow down when n>5. While in Fig.14c and d, the warping stress and shear stress increase exponentially and then slow down for larger diaphragm numbers.

(2) As aforementioned in Section 'Verifications with FEA', the effect of the diaphragm thickness on four quantities increases with the diaphragm number. So the diaphragm thickness cannot be ignored for the distortion of cantilever girders with diaphragms, especially when n>3.

6.2. Case II

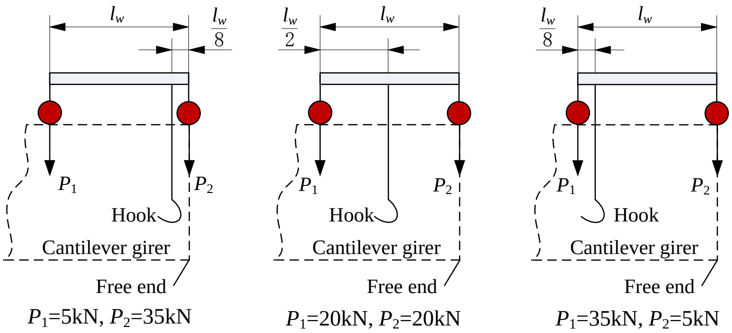

(a) LC1 (b) LC2 (c) LC3

Fig.15 Distribution of eccentric loads caused by the hook's location

In this section, three loading cases LC1~LC3 in Fig.15 are analyzed, where the distribution of eccentric loads caused by the hook's location is fully considered. The location of loads P_1 and P_2 is referred to *Case* I. The distance between two wheels is l_w, and l_w=0.1l. The total hook's force is 40kN. In LC1, the hook is located at one eighth of l_w away from the right wheel, and P_1=5kN and P_2=35kN. In LC2, the hook is located symmetrically , and P_1=P_2=20kN. In LC3, the hook is located at one eighth of l_w away from the left wheel, and P_1=35kN and P_2=5kN.

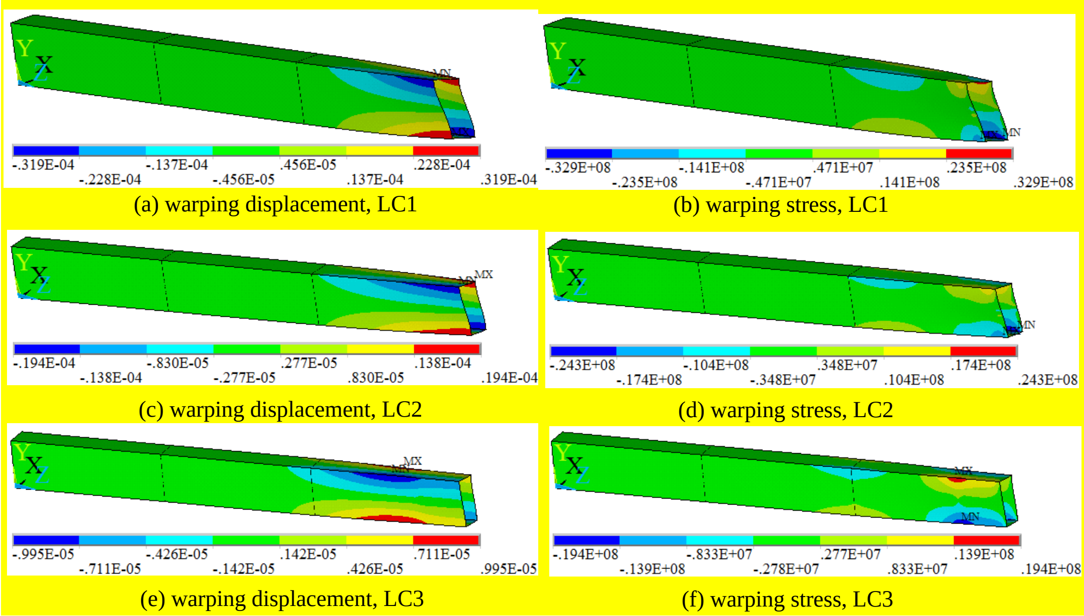

(a) warping displacement, LC1 (b) warping stress, LC1

(c) warping displacement, LC2 (d) warping stress, LC2

(e) warping displacement, LC3 (f) warping stress, LC3

Fig.16 3D contours of warping displacements and stresses for cantilever girders with two diaphragms under LC1~LC3 (amp=100)

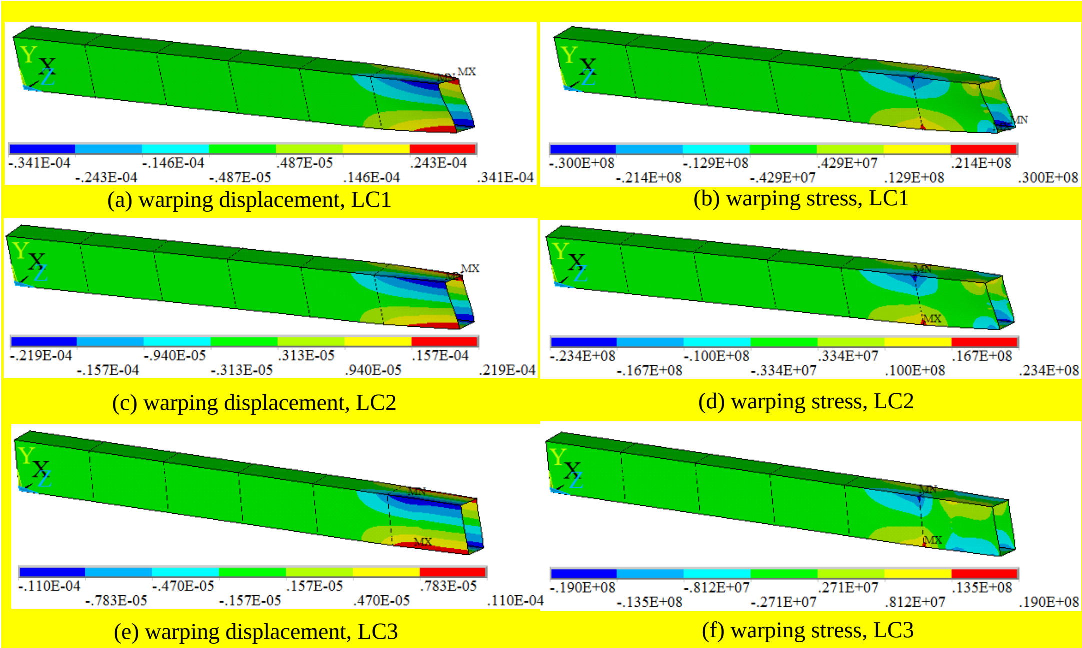

(a) warping displacement, LC1 (b) warping stress, LC1

(c) warping displacement, LC2 (d) warping stress, LC2

(e) warping displacement, LC3 (f) warping stress, LC3

Fig.17 3D contours of warping displacements and stresses for cantilever girders with five diaphragms under LC1~LC3 (amp=100)

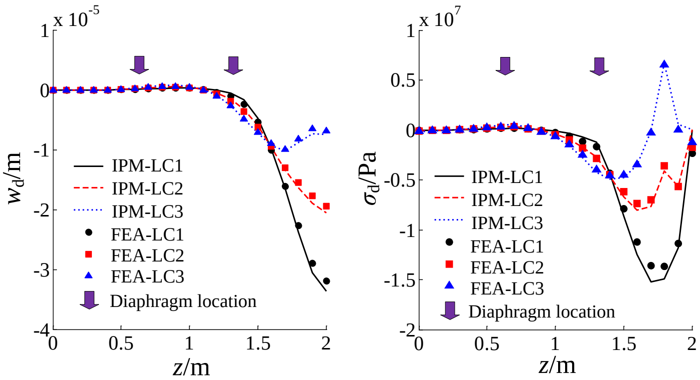

(a) warping displacement (b) warping stress

Fig.18 Distribution of (a) warping displacement and (b) warping stress of the cantilever girder with two diaphragms under LC1~LC3

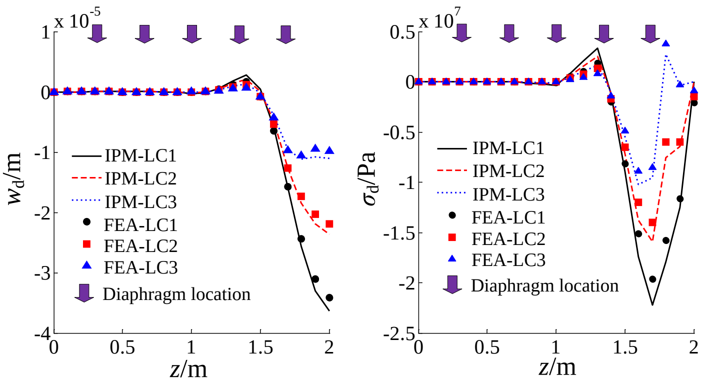

(a) warping displacement (b) warping stress

Fig.19 Distribution of (a) warping displacement and (b) warping stress of the cantilever girder with five diaphragms under LC1~LC3

Fig.16~Fig.17 give the 3D contours of distortional warping displacements and stresses for cantilever box girders with 2 and 5 diaphragms under LC1~LC3, respectively. The 'amp' indicates the amplified factor of deformations. In FEA model, Young's modulus E=2.1×10^{11}Pa, Poisson's ratio υ=0.3, the span l=2m, the width b=0.1m, the height h=0.2m and the flanges and webs thicknesses t_1=t_2=t_3=0.01m. Diaphragms are distributed uniformly along the span with t_p=0.005m.

Comparison results between FEA and IPM are shown in Fig.18 and Fig.19 for warping displacements and stresses for cantilever girders with 2 and 5 diaphragms under LC1~LC3.

Some findings can be drawn from Fig.18 and Fig.19 as follows

(1) The IPM results show good agreements with the FEA ones for the distortional warping stresses and displacements. Besides, the warping stresses and displacements in LC2 are right the average of those in LC1 and LC3 due to the linear superposition.

(2) The distribution of loads P_1 and P_2 will influence the position and value of maximum warping displacement and stress. For girders with 2 diaphragms, when the hook moves from the right (LC1) to left (LC3), the maximum warping displacement reduces from 33.7μm to 10.2μm and the corresponding position changes from the free end to the section z=1.7m; meanwhile, the maximum warping compressive stress reduces from 15.2Mpa to 4.93Mpa and the position from the section z=1.7m to z=1.4m. While for girders with 5 diaphragms, the maximum displacement reduces from 36.3μm to 11.2μm and the position changes from the free end to the section z=1.8m; meanwhile, the maximum warping compressive stress reduces from 22.2Mpa to 10.2Mpa and the position from the section z=1.7m to z=1.6m.

(3) Both the maximum warping displacement and compressive stress in LC3 are the smallest among all LCs. However, the maximum tensile stress in LC3 is 36% larger than the compressive one for girders with 2 diaphragms, which may result in the crack propagation when there is crack in the tensile field. It will be effective to reduce the tensile stress by installing more diaphragms. As shown in Fig.19b, the maximum tensile stress get reduced to 2.74Mpa for girders with 5 diaphragms in LC3, taking only 40.96% of those for girders with 2 diaphragms.

So the warping displacements, the compressive and tensile stresses should be all taken into account when choosing the reasonable hook's location for cantilever girders with diaphragms.

6.3. Case III

The distortional warping stresses and displacements at node N for the sections z=0.05l, 0.5l and 0.95l are analyzed with the trolley moving from the fixed end to the free one for cantilever girders with 2 and 5 diaphragms in LC2, where the measurements for both the section and diaphragms are referred to *Case* II. The influence lines for warping stresses and displacements are analyzed in Fig.20 to Fig. 22 in terms of the sections z=0.05l, 0.5l and 0.95l.

Fig.20 shows the influence lines for warping stresses and displacements at the section z=0.05l varying with the position z_1 of the left wheel for cantilever girders with and without diaphragms in LC2. It is seen that the minimum values occur at z_1=0.15l for warping stresses (Fig.20a) and z_1=0.1l for the displacements (Fig. 20b). Compared with the girder without diaphragms, the minimum warping stress gets reduced by 24.3% for girders with 2 diaphragms and 87.3% for girders with 5 diaphragms, while for warping displacements, the percentages are 10.7% and 72.1%. Besides, all curves converge to zero after z_1=0.6l.

Fig.21 gives the case of the cross section z=0.5l for the warping stresses and displacements in LC2. It shows that the warping stress is approximately symmetrical to z_1=0.45l in Fig.21a. The maximum stress occurs at around z_1=0.4l and z_1=0.5l for girders without diaphragms and with 2 diaphragms. While for the warping displacement in Fig.21b, it shows anti-symmetry to z_1=0.45l.

Both the warping stresses and displacements are largely restrained by more diaphragms.

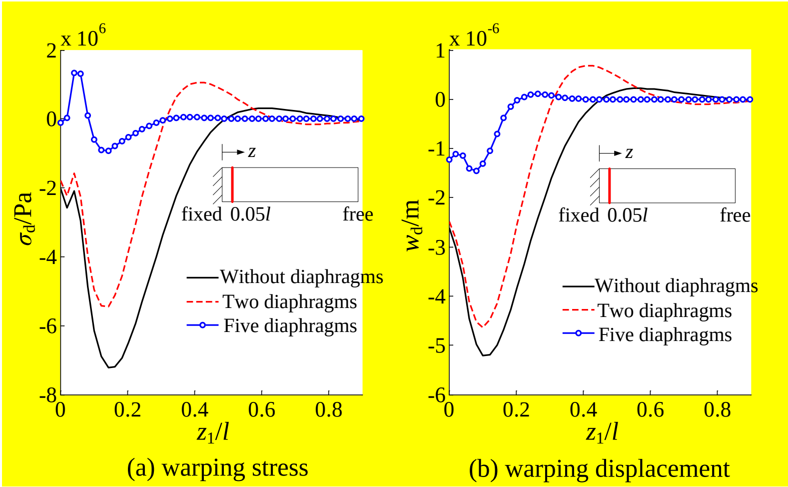

Fig.20 Influence lines of warping stresses and displacements of the cross section z=0.05*l* for cantilever girders without and with diaphragms under moving wheel loads

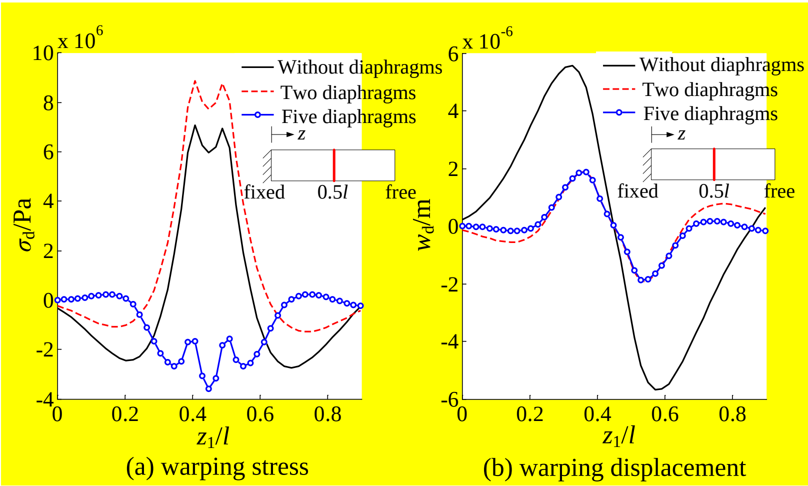

Fig.21 Influence lines of warping stresses and displacements of the cross section z=0.5*l* for cantilever girders without and with diaphragms under moving wheel loads

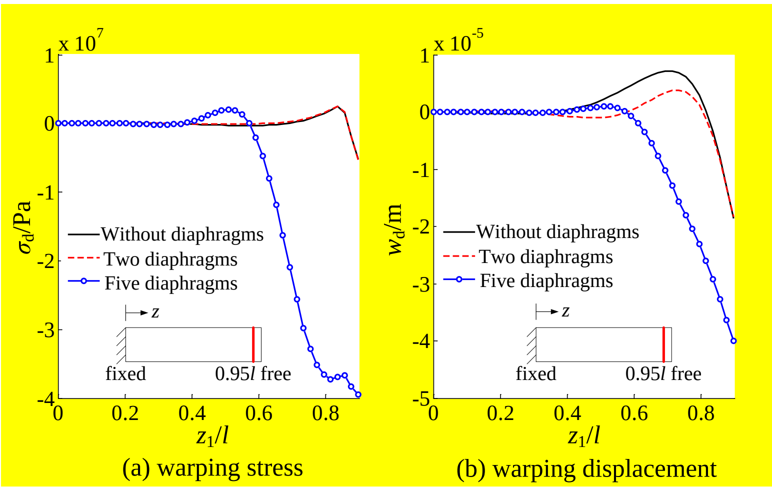

Fig.22 Influence lines of warping stresses and displacements of the cross section z=0.95*l* for cantilever girders without and with diaphragms under moving wheel loads

Fig.22 shows the influence lines of the cross section z=0.95l for the warping displacements and stresses in LC2. For the warping stresses in Fig.22a, it shows a big drop after the critical position around z_1=0.3l for girders with 5 diaphragms and z_1=0.6l for those without diaphragms and those with 2 diaphragms. While for the warping displacements in Fig.22b, the similar big drop is shown after z_1=0.58l for girders with 2 diaphragms and z_1=0.35l for those without diaphragms and those with 5 diaphragms. Besides, compared with those with 2 diaphragms, girders with 5 diaphragms have a larger increment for both displacements and stresses at the free end.

Based on the analysis, both the loading position and the cross section being concerned should be taken into account when choosing the proper diaphragm number for cantilever girders.

Also, as aforementioned in Section 'IPM solution', the moment M_{pi} is introduced to indicate the interactions between the girder and diaphragms. M_{pi} is believed to be the key point in solving the distortion of cantilever girders with inner flexible diaphragms. So it is necessary to examine the variability of the moment M_{pi} (i=1,2,…,n) under moving wheel loads.

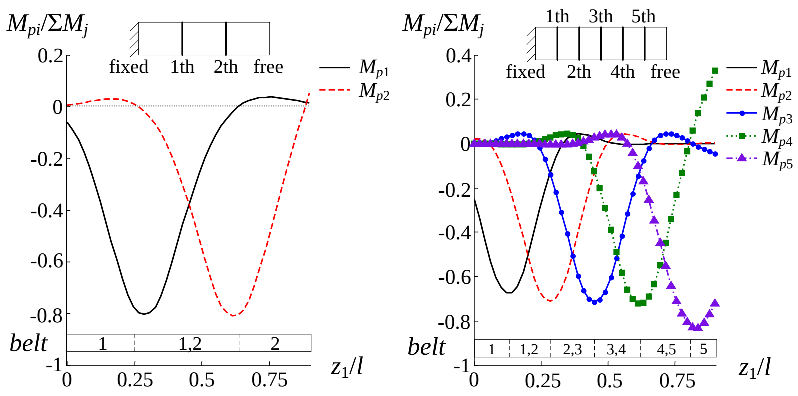

(a) n=2 (b) n=5

Fig.23 Distortional moments M_{pi} of diaphragms for cantilever girders with (a) two and (b) five diaphragms

Fig.23 shows the distortional moments M_{pi} (i=1,2,…,n) of diaphragms for cantilever girders with 2 and 5 diaphragms, where M_j (j=1,2) are the external moments produced by distortional loads, and M_1=M_2=500Nm and ΣM_j=1000Nm in LC2. The range for the negative moment M_{pi} is defined as 'effective interval' (EI) for diaphragms, since only the M_{pi}, in the direction opposite to M_j, will resist the warping deformation and stresses of the cross section.

It is seen from Fig.23a that the EIs for both M_{p1} and M_{p2} occupy approximately 70 percent of the span for cantilever girders with 2 diaphragms. While the occupations for all M_{pi}s reduce to less than 50 percent for girders with 5 diaphragms in Fig.23b. Besides, several segments are divided in the bottom belt based on EIs, and the numbers in segments indicate the diaphragms with negative M_{pi}. This means: when the trolley moves from the left to right, the 1th diaphragm is the first to resist distortional deformations, followed by both diaphragms in the middle and the 2th diaphragm at last for cantilever girders with 2 diaphragms. The similar process is performed for girders with 5 diaphragms in the order of the 1th, 1th and 2th, 2th and 3th, 3th and 4th, 4th and 5th, 5th diaphragms. Besides, considering the linearity between the moment M_{pi} and the shear strain γ_{pi}, Fig.23 also shows the variability of the shear strain γ_{pi} of diaphragms under moving wheel loads.

7. Conclusions

The distortion of cantilever girders with inner flexible diaphragms subjected to concentrated eccentric loads is investigated using initial parameter method, in which the in-plane shear strain of diaphragms is considered. Based on the compatibility condition between the girder and diaphragms, solutions for distortional warping displacements and stresses are both obtained. The main conclusions can be drawn as follows

(1) Compared with FEA results, the IPM has a high accuracy in calculating the distortional angle, warping displacements and stresses for cantilever girders with inner flexible diaphragms. However, the distortional angle obtained from the IPM is susceptible to the influence of stress concentration, and it is necessary to install more diaphragms at the loading sections.

(2) A series of parametric studies are performed to examine the effects of the diaphragm number and thickness, the ratio of height to span of the girder, the hook’s location and the wheels' positions on the distortion of cantilever girders with inner diaphragms.

In Case I, four quantities - distortional angle, warping displacement and stress, shear stress all vary exponentially along with the diaphragm number under various ratios h/l and t_p/t. The effect of the diaphragm thickness on four quantities increases with the diaphragm number and cannot be ignored when the diaphragm number exceeds 3.

In Case II, the distribution of eccentric loads influences the positions and values of maximum warping displacement and stress. The maximum compressive stress in LC3 is the smallest among all LCs, but the tensile stress is the largest, which may result in the crack propagation when there is a crack in the tensile field. It would be effective to lower the tensile stress by installing more diaphragms.

In Case III, a series of influence lines of distortional warping stresses and displacements are obtained at node N for the cross sections z=0.05l, 0.5l and 0.95l for cantilever girders with 2 and 5 diaphragms under moving wheel loads. The influence lines of displacements and stresses are related to the number of diaphragms and the position of cross section being analyzed. Results show that both the loading position and the cross section being concerned should be taken into account when choosing the proper diaphragm number for cantilever girders.

Based on the initial parameter method, it is possible to optimize the warping displacements and stresses of cantilever girders considering the position and thickness of diaphragms. The future work will be extensively researched for (1) the optimization of warping displacement and stress, (2) the distortion of cantilever girders with perforated diaphragms.

Acknowledgements

This work is supported by the National Natural Science Foundation of China (NSFC) [grant number: 51175442 , 51675450].

Appendix A

The relationships between $\varphi_i(z)$ (i=1,2,3,4) and their differentiations are

$$\varphi_1^{(1)} = \lambda_1\varphi_4 + \lambda_2\varphi_2\,,\ \ \varphi_2^{(1)} = \lambda_1\varphi_3 - \lambda_2\varphi_1\,,\ \ \varphi_3^{(1)} = \lambda_1\varphi_2 - \lambda_2\varphi_4\,,\ \ \varphi_4^{(1)} = \lambda_1\varphi_1 + \lambda_2\varphi_3\,; \qquad \text{(A.1)}$$

$$\varphi_1^{(2)} = \left(\lambda_1^{\,2} - \lambda_2^{\,2}\right)\varphi_1 + 2\lambda_1\lambda_2\varphi_3\,,\ \ \varphi_2^{(2)} = \left(\lambda_1^{\,2} - \lambda_2^{\,2}\right)\varphi_2 - 2\lambda_1\lambda_2\varphi_4\,,$$

$$\varphi_3^{(2)} = \left(\lambda_1^{\,2} - \lambda_2^{\,2}\right)\varphi_3 - 2\lambda_1\lambda_2\varphi_1\,,\ \ \varphi_4^{(2)} = \left(\lambda_1^{\,2} - \lambda_2^{\,2}\right)\varphi_4 + 2\lambda_1\lambda_2\varphi_2\,; \qquad \text{(A.2)}$$

$$\varphi_1^{(3)} = \left(\lambda_1^{\,3} - 3\lambda_1\lambda_2^{\,2}\right)\varphi_4 + \left(3\lambda_1^{\,2}\lambda_2 - \lambda_2^{\,3}\right)\varphi_2\,,\ \ \varphi_2^{(3)} = \left(\lambda_1^{\,3} - 3\lambda_1\lambda_2^{\,2}\right)\varphi_3 - \left(3\lambda_1^{\,2}\lambda_2 - \lambda_2^{\,3}\right)\varphi_1\,,$$

$$\varphi_3^{(3)} = \left(\lambda_1^{\,3} - 3\lambda_1\lambda_2^{\,2}\right)\varphi_2 - \left(3\lambda_1^{\,2}\lambda_2 - \lambda_2^{\,3}\right)\varphi_4\,,\ \ \varphi_4^{(3)} = \left(\lambda_1^{\,3} - 3\lambda_1\lambda_2^{\,2}\right)\varphi_1 + \left(3\lambda_1^{\,2}\lambda_2 - \lambda_2^{\,3}\right)\varphi_3\,. \qquad \text{(A.3)}$$

References

[1] A.H. Siddiqui, S.F. Ng, Effect of diaphragms on stress reduction in box girder bridge sections,

Can. J. Civ. Eng. 15 (1987) 127-135.

[2] T. Green, N. Yazdani, L. Spainhour, Contribution of intermediate diaphragms in enhancing precast bridge girder performance, J. Perform Constr. Facil. 18 (2004) 142-146.

[3] R.N. Wright, S.R. Abdel-Samad, A.R. Robinson, BEF analogy for analysis of box-girders, J. Struct. Div. 94 (1968) 1719-1743.

[4] Y.T. Hsu, D.R. Schelling, EBEF method for distortional analysis of steel box-girder bridges, J. Struct. Eng. 121 (1995) 557-66.

[5] Y.T. Hsu, C.C. Fu, Application of EBEF method for the distortional analysis of steel box girder bridge superstructures during construction, Adv. Struct. Eng. 5 (2002) 211-221.

[6] L.F. Boswell, Q. Li, Consideration of the relationships between torsion, distortion and warping of thin-walled beams, Thin-Walled Struct. 21 (1995) 147-161.

[7] Q. Li, Investigation of the warping functions of thin walled bars with closed cross section. J. Southwest Jiaotong Univ. 6 (1993) 1-6.

[8] Z.M. Zhao, Z.Z. Fang, J.Q. Guo, Analysis of continuous box girders with diaphragms by finite strip method, Bridge Constr. 4 (1993) 35-53.

[9] J.S. Ye, J. Zhang, X.M. Zhao, Kalman filtering identification for displacement parameters of continuous curved box girder bridge based on novozhilov flexibility theory, China J. Highway Transport. 20 (2007) 65-69.

[10] J. Zhang, J.S. Ye, X.M. Zhao, Dynamic Bayesian stochastic estimation to displacement parameters of continuous curved box with segregating slab, Chinese J. Appl. Mech. 24 (2007) 69-74.

[11] X.T. Chu, Z.M. Ye, L.Y. Li, Local and distortional buckling of cold-formed zed-section beams under uniformly distributed transverse loads, Int. J. Mech. Sci. 48 (2006) 378-388.

[12] Z.M. Zhao, The calculating analysis for multiple span continuous curved box girder by the finite strip method, J. Fuzhou Univ. (N. Sci.) 25 (1997) 90-94.

[13] Z.M. Zhao, Analysis of continuous curved box-girder bridge with flexible transverse diaphragms by finite strip method, Comp. Struct. Mech. Appl. 10 (1993) 473-484.

[14] Y. Suetake, M. Hirashima, Extended trigonometric series analysis of box girders with diaphragms, J. Eng. Mech. 123 (1997) 293-301.

[15] N.H. Park, N. Lim, Y. Kang, A consideration on intermediate diaphragm spacing in steel box girder bridges with a doubly symmetric section, Eng. Struct. 25 (2003) 1665-1674.

[16] N.H. Park, Y. Choi, G. Yi, Distortional analysis of steel box girders, Steel Struct. 2 (2002) 51-58.

[17] H.F. Li, Y.F. Luo, Application of stiffness matrix of a beam element considering section distortion effect, J. Southeast Univ. 26 (2010) 431-435.

[18] N.H. Park, Y. Choi, Y. Kang, Spacing of intermediate diaphragms in horizontally curved steel box girder bridges, Finite Elem. Anal. Des. 41 (2005) 925-943.

[19] J.H. Lee, S.K. Lee, J.H. Lim. Spacing of intermediate diaphragms horizontally curved steel box girder bridges considering bending-distortional warping normal stress ratio, J. Korea Acad-Ind. coorp. Soc. 16 (2015) 6325-6332.

[20] Y.J. Choi, N.H. Park, S.S. Hong, A consideration on intermediate diaphragm spacing of horizontally curved steel box girders, J. Korean Sco. Civ. Eng. 23 (2003) 345-353.

[21] N.H. Park, S. Choi, Y. Kang, Exact distortional behavior and practical distortional analysis of multicell box girders using an expanded method, Comp. Struct. 83 (2005) 1607-1626.

[22] N.H. Park, Y.J. Kang, H.J. Kim, An independent distortional analysis method of thin-walled multicell box girders, Struct. Eng. Mech. 21 (2005) 275-293.

[23] N.H. Park, K.Y. Yoon, S.K. Cho, Effective distortional stiffness ratio and spacing of intermediate diaphragms in steel box girder bridges, Steel Struct. 4 (2004) 93-102.

[24] A. Saber, W. Alaywan, Full-scale test of continuity diaphragms in skewed concrete bridge girders, J. Bridge Eng. 16 (2011) 21-28.

[25] R.E. Abendroth, F.W. Klaiber, M.W. Shafer, Diaphragm effectiveness in prestressed-concrete girder bridges, J. Struct. Eng. 121 (1995) 1362-1369.

[26] Y. Sieffert, G. Michel, P. Ramondenc, Effects of the diaphragm at midspan on static and dynamic behavior of composite railway bridge: a case study, Eng. Sturct. 28 (2006) 1543-1554.

[27] W.H. Dilger, G.A. Ghoneim, G.S. Tadros, Diaphragms in skew box girder bridges, Can. J. Civ. Eng. 15 (1988) 869-878.

[28] I. Mohseni, A.K.A. Rashid, J. Kang, Effect of intermediate diaphragm on lateral load distribution factor of multicell box-girder bridges, KSCE J. Civ. Eng. 18 (2014) 2128-2137.

[29] V.Z. Vlasov, Thin walled elastic beams, Second ed., Israel Program for Scientific Translations, Israel, 1961.

[30] X. Xu, S.Z. Qiang, Research on distortion analysis theory of thin-walled box girder, Eng. Mech. 30 (2013) 192-201.

[31] X. Xu, H.W. Ye, S.Z. Qiang, Distortional analysis of thin-walled box girder taking account of shear deformation, Chin. J. Comp. Mech. 30 (2013)860-866.

[32] M. Harashima, K. Usugi, Distortional analysis of random box girders considering the shear deformation, Foreign Bridge. 1 (1980) 1-29.

[33] J.Q. Guo, Z.Z. Fang, Z. Zheng, Design theory of box girder, Second ed., China Communications Press, Beijing, 2008.